Thermal Stability and Morphological Transformations of $Au_{core}-Co_{shell}$ Nanocrucibles

Tianlong Wen and Kannan M. Krishnan*

Department of Materials Science and Engineering, University of Washington, Box 352120, Seattle, Washington 98195-2120

Received: June 11, 2010; Revised Manuscript Received: July 29, 2010

$Au_{core}-Co_{shell}$ nanoparticles were synthesized by a wet-chemical method in organic solvent and their thermal stability was studied by annealing experiments over a wide temperature range (200−450 °C). During heating, atoms within the core−shell nanoparticles migrate to transform their initial core−shell morphology to a stable "peanut" structure. We show that this morphological transformation occurs by a well-defined series of energy minimization steps that sequentially reduce the energy due to intraphase grain boundaries within the cobalt shell, the interface energy between the gold core and the cobalt shell, and the overall strain energy.

Introduction

In nanoscience and nanotechnology, the thermal properties unique to nano scale materials, compared to their bulk counterpart, continue to be of fundamental interest.[1] In general, these unique thermal properties arise from the significant role played by surfaces and interfaces on the nanoscale. In effect, the break in symmetry at newly created surfaces and interfaces introduces extra energy and entropy terms into the free energy of nanoscale materials and thus alters their thermal properties.[1−4] For example, it has been observed[5] that the premelting of metal surfaces occurs well below the bulk melting point ($T_{M\text{-}B}$), and the thickness of the premelting layer, slowly increasing initially, will dramatically increase to completely melt when approaching $T_{M\text{-}B}$ from low temperature. In fact, because of premelting at the free surface or incoherent interface, the melting phenomenon, commonly a first-order phase transformation in the bulk, may be observed to be of second order at the nanoscale.[6,7] As a result, the melting temperature of nanoparticles having free surfaces or incoherent interfaces with the matrix are depressed;[8,9] in contrast, premelting is not observed in nanoparticles having a coherent interface with the matrix, and such nanoparticles melt above $T_{M\text{-}B}$.[9]

While there are many theoretical predictions of the thermal properties of nanoparticles,[2−4,10−14] only a few experiments have been conducted. The stability of thermally heated single-component nanoparticles[15−18] and two-component miscible systems[19] has been investigated by in situ transmission electron microscopy (TEM), and the main conclusion drawn from these heating experiments is that nanoparticles coalesce during heating to reduce their surface energy. Most notably, the size-dependent spontaneous alloying of $Au_{core}-Ag_{shell}$ nanoparticles mediated by vacancies was observed at room temperature to reduce the interface energy.[20] In general, these research works focused on thermal stability in systems exhibiting interparticle interactions and/or miscible alloying systems. However, the thermal stability of a two-component, immiscible, nanoparticle system consisting of a core−shell morphology has not yet been studied. Such a system is unique because it allows one to investigate the thermal stability and the interplay of the two immiscible components during heating without mass exchange between the different core−shell nanoparticles and in which surface, interfacial, grain boundary, and strain energies will determine the thermal behavior and final morphology of each isolated particle. We suggest that these two-component nanoparticles, isolated by a layer of surfactant on their surface and characterized by no interparticle interaction, behave as "nanocrucibles". Here, we discuss annealing experiments carried out on immiscible $Au_{core}-Co_{shell}$ nanoparticles to investigate the thermal stability of these nanocrucibles and specifically to determine the role of various energies (surface, interface, grain boundary and strain) in their thermal behaviors (interparticle coalescence is not discussed here but in Figure S1 of Supporting Information). With respect to the atoms in the bulk undistorted lattice, surface, interfacial, grain boundary, and strain energy refers to the increase of free energy due to incomplete coordination of neighboring atoms at bare surface (surface), atomic and chemical disorder at the interface between two phases (interface), misorientation of two crystallites of the same phase (grain boundary), and lattice distortion of adjacent phases associated with lattice mismatch (strain), respectively.[21] Magnitude of surface energy is a function of crystallographic orientation of the bare surface; interfacial energy is a function of the relative crystallographic orientations of adjacent *interphase* crystallites; grain boundary energy is function of relative crystallographic orientation of *intraphase* crystallites; strain energy is a bulk energy with magnitude determined by volume of distorted area, degree of lattice distortion, and Young's modulus.[21]

Experimental Methods

Chemicals. Octacarbonyldicobalt ($Co_2(CO)_8$, stabilized with 1−5% hexane) was purchased from Alfa Aesar and is kept below −25 °C in a freezer in a glovebox to prevent decomposition and oxidation. Gold(III) chloride hydrate ($HAuCl_4$, 99.999%), tetraoctylammonium bromide (TOAB, 98%), oleic acid (OA, ≥99%), oleylamine (ON, 70%), dodecylamine (DDA, 98%), and toluene (99.8%, anhydrous) are purchased from Sigma-Aldrich and also kept under the argon atmosphere in a glovebox. Sodium borohydride ($NaBH_4$, 99%) was purchased from Sigma-Aldrich and stored in ambient condition. All chemicals are used without further treatment.

Synthesis of $Au_{core}-Co_{shell}$ Nanoparticles. The gold precursor nanoparticles were synthesized by a two-phase reduction of phase-transferred $AuCl_4^-$ by sodium borohydride in the

* To whom correspondence should be addressed. E-mail: kannanmk@uw.edu.

10.1021/jp1053666
Published on Web 08/13/2010

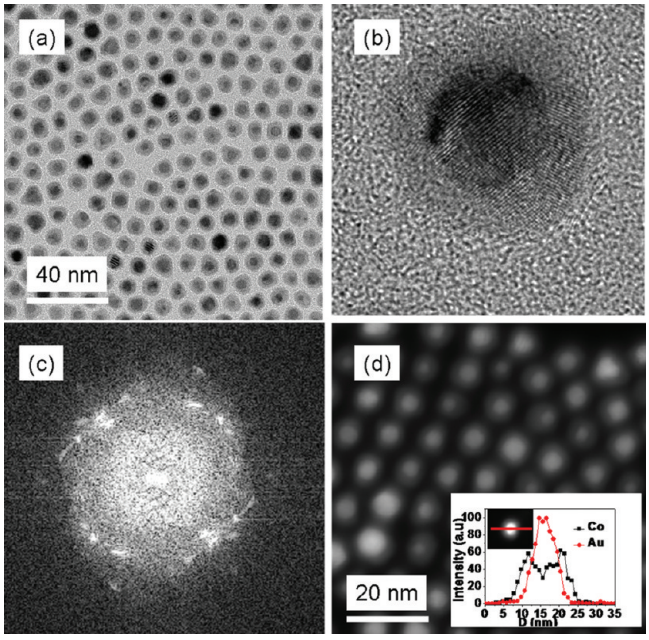

Figure 1. Bright-field TEM, HRTEM, and dark-field STEM images of as-synthesized Au_{core}-Co_{shell} nanoparticles in (a), (b), and (d) respectively, and (c) the FFT of the core−shell particles in (b). The inset in (d) shows the representative EDX line scan, with probe size ~1 nm, clearly establishing the chemical $Au_{core}-Co_{shell}$ morphology of the nanoparticles.

presence of a linear amine.[22] The gold precursor nanoparticles, coated with amine as surfactant, were washed with methanol, precipitated by centrifuge, dried in vacuum, and then redispersed in toluene to make gold precursor solutions. The gold precursor solution containing 0.05 g of gold nanoparticles was degassed by Argon for 30 min in a three-neck flask, then heated up to 90 °C, and followed by injection of 0.1 g of $Co_2(CO)_8$ in 3 mL of toluene with presence of extra surfactant. As $Co_2(CO)_8$ slowly decompose to cobalt atoms, they preferentially coat the surface of gold precursor nanoparticles to form $Au_{core}-Co_{shell}$ nanoparticles due to the lower activation energy of heterogeneous nucleation than homogeneous cobalt nucleation.[23−26] The synthesized $Au_{core}-Co_{shell}$ nanoparticles dispersed in toluene were collected and sealed in vials filled with argon gas, and then stored in a glovebox to prevent oxidation.

Ex Situ Heating Experiment. For annealing experiments, a small drop of the $Au_{core}-Co_{shell}$ nanoparticles solution was put on a carbon film mounted on a copper grid. The carbon film was chosen because carbon is immiscible in both gold and cobalt below 500 °C[27] (see Figure S2 in Supporting Information). The nanoparticle-coated copper grid was then placed in a quartz tube furnace (see Scheme S1 in Supporting Information) to be degassed with argon gas for 2 h before slowly heating up. After that, the $Au_{core}-Co_{shell}$ nanoparticles on the TEM grids were heated up to 200, 250, 300, 350, 400, and 450 °C, respectively, kept at these temperature for 10 h and then allowed to cool down to room temperature. Besides the $Au_{core}-Co_{shell}$ nanoparticles, pure cobalt nanoparticles were also heat treated under the same conditions as control samples. Finally, these heat treated $Au_{core}-Co_{shell}$ and cobalt nanoparticles were characterized at room temperature by TEM, scanning transmission electron microscopy (STEM), energy dispersive X-ray spectroscopy (EDX), and selected area electron diffraction (SAED) using a FEI Tecnai G2 F20 microscope operated at 200 kV.

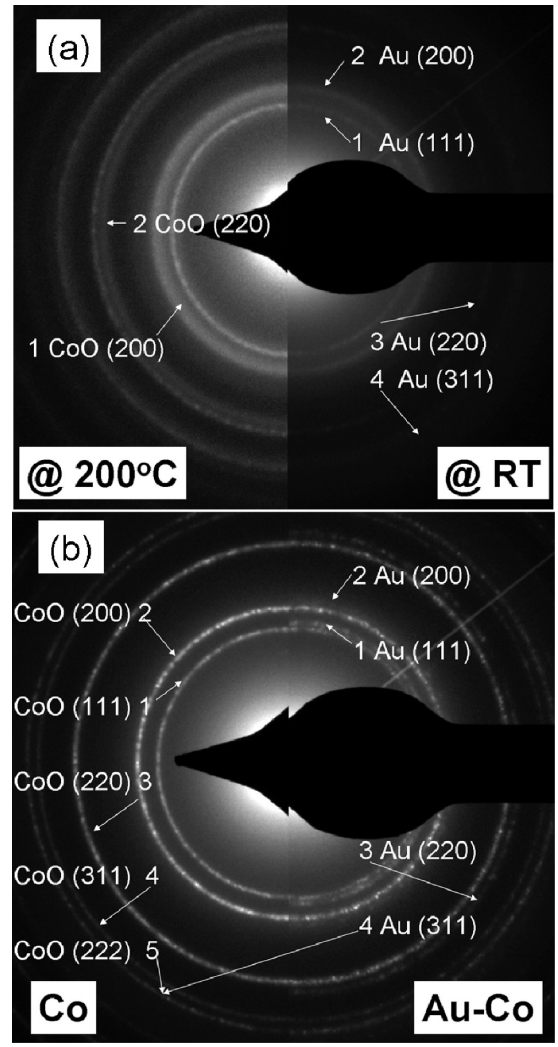

Figure 2. The SAED of $Au_{core}-Co_{shell}$ nanoparticles. (a) As-synthesized (right half) and heat treated at 200 °C (left half) and (b) cobalt (left half) and $Au_{core}-Co_{shell}$ nanoparticles (right half) heated treated at 250, 300, 350, and 400 °C in (b).

Results and Discussion

The bright-field TEM and dark-field STEM images of as-synthesized $Au_{core}-Co_{shell}$ nanoparticles are shown in parts a and d of Figure 1. The gold cores and cobalt shells are easily distinguished in both bright-field TEM images and dark-field STEM images due to their atomic number or Z contrast; the cores appear darker (or lighter in dark field STEM), and the shells appear lighter (or darker). The chemical morphology of the as-synthesized $Au_{core}-Co_{shell}$ nanoparticles is further confirmed by the EDX line scan profile, using a 1 nm probe in STEM mode, as shown in the inset of Figure 1d. Figure 1b shows a high-resolution TEM (HRTEM) image of the as-synthesized $Au_{core}-Co_{shell}$ nanoparticles. It can be seen from the HRTEM image that the gold core is a single crystal and is enclosed by multiple grains of the cobalt shell, confirming the heterogeneous nucleation.[23,28] The fast Fourier transform (FFT) of the $Au_{core}-Co_{shell}$ nanoparticle image, shown in Figure 1c, confirms the polycrystalline nature of the as-synthesized core−shell nanoparticles; the FFT shows a complex cobalt signature with multiple grain orientations, unlike the heat treated nanoparticles discussed later. In addition, as-synthesized $Au_{core}-Co_{shell}$ nanoparticles are superparamagnetic with blocking temperature T_B ~225 K, indicating spins in the cobalt shell are

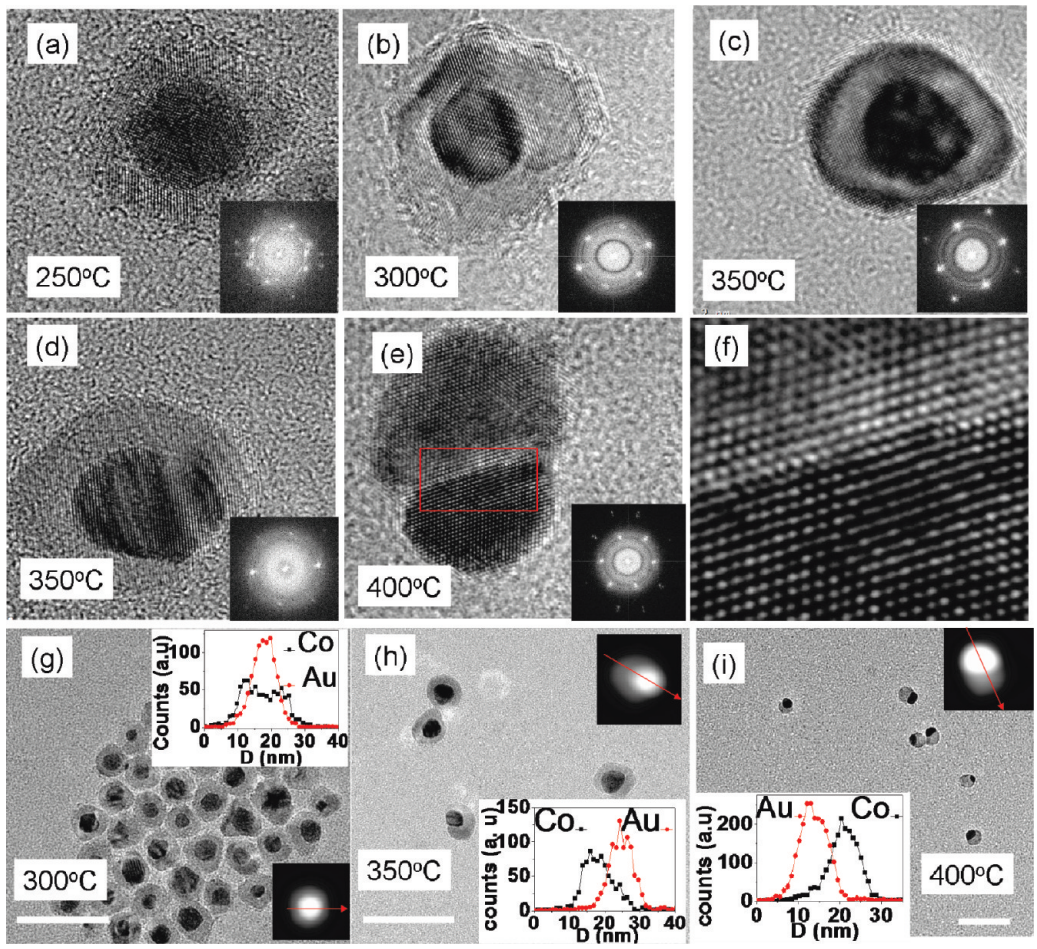

Figure 3. High-resolution TEM of $Au_{core}-Co_{shell}$ nanoparticles heat treated at 250 °C (a), 300 °C (b), 350 °C (c and d), and 400 °C in (e); the FFT of each individual particle is shown as insets. The interface enclosed by the red rectangular area in (e) is magnified and shown in (f). The bright-field TEM image of Au−Co nanoparticles heat treated at 300 °C in (g), 350 °C in (h), and 400 °C in (i); the scale bar is 40 nm. The inset shows the corresponding STEM image of $Au_{core}-Co_{shell}$ nanoparticles heat treated and the associated EDX line scans with probe size ~1 nm.

aligned by exchange interaction to form single magnetic domains (see Figure S3 in Supporting Information).

The crystal structures of the as-synthesized and heat-treated $Au_{core}-Co_{shell}$ nanoparticles were monitored by SAED as shown in Figure 2. For as-synthesized nanoparticles (Figure 2a, right half), only the diffraction pattern of the gold core is observed with no discernible diffraction features from cobalt due to the small size of cobalt grains. Prior to annealing, no oxidation can be detected for these as-synthesized core−shell nanoparticles either by EDX line scans or SAED. Further, careful degassing of the quartz tube with argon for 2 h prior to annealing ensured that the cobalt was not oxidized during heating/annealing. However, it is known that when heated in an argon atmosphere at high temperature for 10 h, the surfactant on the surface of the cobalt shell will gradually evaporate or decompose[29,30] to leave an exposed metal surface. As a result, even at room temperature, the cobalt nanoparticle surface can oxidize quickly, due to insufficient protection, while being transferred in air to the TEM. Despite such oxidation, however, the morphological transformations arising from the annealing will remain unchanged. Generally, surfactant coverage decreases with increasing annealing temperature. Hence, the SAED pattern shows no surface oxidation of the $Au_{core}-Co_{shell}$ nanoparticles when annealed at temperatures below 200 °C for 10 h; signs of oxidation appear at the surface when $T_{anneal} = 200$ °C, indicated by the appearance of blurred and widened diffraction rings attributed to CoO (200), (220) (left half of Figure 2a). Oxidation proceeds rapidly for samples annealed at even higher temperatures. For $T_{anneal} > 250$ °C (right half of Figure 2b), clear diffraction rings attributed to CoO are visible. It should be reiterated that this oxidation occurs subsequent to the annealing, during specimen transfer to the TEM and therefore has no bearing on the interpretations of the morphological transformations that occur during heating.

During heat treatment, several vital energies determine the stability and final morphology of these $Au_{core}-Co_{shell}$ "nanocrucibles", including the surface energy of the outermost layer of the nanoparticles, the interfacial energy between gold and cobalt, the strain energy in both the core and shell, and the grain boundary energy of the cobalt shell. For chemically synthesized nanoparticles in an organic solvent, each surface atom is coordinated by a functional group of a surfactant with a hydrophobic chain tail. If the interface between the outermost atomic layer of the nanoparticles and the functional group of the surfactant is defined as the "surface" of the core−shell nanoparticles, the "surface energy" of the $Au_{core}-Co_{shell}$ nanoparticles will be negligibly small or even negative due to the very stable coordination bonding between the outermost metal atoms and the functional groups. Furthermore, the surface atoms will be covalently bound to residual carbon atoms[15,29,30] after the surfactants on the surface are evaporated/decomposed. As a result, the dominant mechanism to stabilize the $Au_{core}-Co_{shell}$ nanoparticles is to reduce the sum of the interfacial energy between gold and cobalt (interphase interfacial energy), the

strain energy and the grain boundary energy of cobalt (intraphase interfacial energy).

At the gold−cobalt interface, three possible interactions determine the effective energy;[21] the first possibility is a completely coherent interface, where the lattices of gold and cobalt match perfectly so that they are continuous across the interface. In this case, the only contribution to the interface energy is due to different chemical species on either side of the interface, namely, the interface energy, $\gamma = \gamma_{chem}$, whose value is usually very small (~200 mJ m^{-2}).[21] The second possibility is a semicoherent interface to reduce the strain by introducing misfit dislocations; as a result, the interface energy has contribution from misfit dislocations, i.e., $\gamma = \gamma_{chem} + \gamma_{dis}$ (~200−500 mJ m^{-2}).[21] The third possibility is an incoherent interface with great atomic disorder, usually with a very large (>500 mJ m^{-2})[21] interface energy. Of the three possibilities, a coherent or semicoherent interface (or some low energy interface) is favored to reduce the interfacial energy of the $Au_{core}-Co_{shell}$ nanoparticles. The strain energy stored in the core and shell, proportional to the volume of the core, can be estimated by the Eshelby's inclusion[31] model in which a particle is embedded in an infinite bulk matrix, namely, $E_S = 2\,\mu V\varepsilon^2(1+\sigma)/9(1-\sigma)$, where μ, ε, σ, and V are the shear modulus, strain, Poisson's ratio, and volume of core, respectively. A rough estimation of the strain energy stored in the gold core and cobalt shell is approximately equal to the total energy of the disordered interface for $Au_{core}-Co_{shell}$ nanoparticles (for accurate calculation of core−shell nanoparticles, please refer to ref 32). Finally, the intraphase grain boundary in the cobalt shell is energetically unfavorable, and the system will eliminate these grain boundaries generated by heterogeneous nucleation.

As shown in Figure 1, the cobalt shell of the $Au_{core}-Co_{shell}$ nanoparticles is comprised of multiple grains, resulting in extra grain boundary energy. During heat treatment, even at temperatures as low as 250 °C, atomic diffusion anneals out the grain boundaries, as shown in Figure 3a, and is supported by the more regular FFT in the inset. Such grain growth at intermediate temperature is known to be driven by the grain boundary enthalpy and the enhanced grain boundary mobility due to nonequilibrium grain boundary structures in nanocrystalline materials.[33] At the same time, the lattices of the gold core and the cobalt shell reorient such that a coherent or semicoherent interface can be obtained. This reorientation of the gold core and cobalt shell lattices and elimination of the grain boundaries in the cobalt shell are observed in the HRTEM image for the core−shell nanoparticles heat treated at 300 °C for 10 h as shown in Figure 3b. The representative FFT of the image in Figure 3b shows a regular pattern, indicating the disappearance of grain boundaries of the cobalt shell and the alignment of the lattices of the gold core and cobalt shell. At higher temperatures, atoms will gain even more energy to allow them to migrate/diffuse more vigorously. As a result, annealing at 350 °C for 10 h (Figure 3d) causes the physical extent of the gold/cobalt interface to be reduced by movement of the gold cores out from containment within the cobalt shell, and into the "environment". However, even during this process, the lattice coherency is maintained as indicated by the inset FFT in Figure 3d. By this movement, the gold/cobalt interface is gradually reduced along with some strain energy being relaxed. Annealing at even higher temperatures (400 °C) accelerates the movement process, with the $Au_{core}-Co_{shell}$ nanostructures finally morphing into a peanut structure as shown in Figure 3e, with both the interface and strain energies further minimized. Figure 3f shows the twinned semicoherent interface of the peanut structure in Figure 3e. The structure of the nanoparticles remains unchanged after heat treatment at 450 °C (see Figure S5 in Supporting Information), indicating that a final, stable morphology is obtained. This entire process is also consistent with the observation of the bright-field TEM image and the spatially resolved chemical composition analysis by EDX line scans as shown in the insets of parts g−i of Figure 3.

Conclusions

In summary, to minimize their total energy during annealing experiments, $Au_{core}-Co_{shell}$ nanocrucibles follow a sequence of thermal transformations: (1) when thermal energy is low (<200 °C), core−shell morphology is stable, (2) as the temperature increases (200−300 °C), cobalt atoms in the shell begin to diffuse and reorganize to eliminate grain boundaries. Further, the gold and cobalt lattices reorient and align to create a coherent/semicoherent interface; (3) as the annealing temperature is further increased to 350 °C, atoms migrate more vigorously such that the gold core begins to move out from containment within the cobalt shell to reduce the interfacial energy by diminishing contact area and to partially release strain energy as well; and finally, (4) strain, interface and grain boundary energies are minimized to form "peanut" structures for particles heat treated at 400 °C for 10 h. Preliminary in situ TEM heating experiments are consistent with these results.[34]

Acknowledgment. This project was supported by National Science Foundation, DMR No. 0501421. The authors acknowledge Prof. E. A. Stach (Purdue University) for in situ TEM heating experiments. Part of this work was conducted at the UW-NTUF, a member of the NSF-NNIN.

Supporting Information Available: Additional information on X-ray $\theta-2\theta$ scan with Cu Kα radiation of $Au_{core}-Co_{shell}$ nanoparticles, magnetic characterization, TEM images of coalesced nanoparticles, and bulk phase diagrams of Au−Co, Au−C, and Co−C binary systems. This material is available free of charge via the Internet at http://pubs.acs.org.

References and Notes

(1) Baletto, F.; Ferrando, R. *Rev. Mod. Phys.* **2005**, *77*, 371–423.
(2) Hill, T. L. *Thermodynamics of small systems*; Dover: New York, 1994.
(3) Hill, T. L. *Nano Lett.* **2001**, *1*, 273–275.
(4) Hill, T. L. *Nano Lett.* **2001**, *1*, 111–112.
(5) Frenken, J. W. M.; van der Veen, F. F. *Phys. Rev. Lett.* **1985**, *54*, 134–137.
(6) Cahn, R. W. *Nature* **1986**, *323*, 668–669.
(7) Dash, J. G. *Rev. Mod. Phys.* **1999**, *77*, 1737–1743.
(8) Buffat, P.; Borel, J. P. *Phys. Rev. A* **1976**, *13*, 2287–2298.
(9) Jin, Z. H.; Sheng, H. W.; Lu, K. *Phys. Rev. B* **1999**, *60*, 141–149.
(10) Shirinyan, A. S.; Wautelet, M. *Nanotechnology* **2004**, *15*, 1720–1731.
(11) Zhu, Y. F.; Lian, J. S.; Jiang, Q. *J. Phys. Chem. C.* **2009**, *113*, 16896–16900.
(12) Yang, C. C.; Li, S. *J. Phys. Chem. C.* **2008**, *112*, 16400–16404.
(13) Lewis, L. J.; Jensen, P.; Barrat, J. L. *Phys. Rev. B* **1997**, *56*, 2248–2257.
(14) Wautelet, M.; Shirinyan, A. S. *Pure Appl. Chem.* **2009**, *81*, 1921–1930.
(15) Sutter, E.; Sutter, P.; Zhu, Y. *Nano Lett.* **2005**, *5*, 2092–2096.
(16) Palasantzas, G.; Vystavel, T.; Koch, S. A.; De Hosson, J. Th. M. *J. Appl. Phys.* **2006**, *99*, 024307.
(17) Asoro, M. A.; Kovar, D.; Shao-Horn, Y.; Allard, L. F.; Ferreira, P. J. *Nanotechnology* **2010**, *21*, 025701.
(18) Ristau, R.; Tiruvalam, R.; Clasen, P. L.; Gorskowski, E. P.; Harmer, M. P.; Kiely, C. J. *Gold Bull.* **2009**, *42*, 133–143.
(19) Gautam, A. R. S.; Howe, J. M. *J. Mater. Sci.* **2009**, *44*, 601–607.
(20) Shibata, T.; Bunker, B. A.; Zhang, Z.; Meisel, D.; Vardeman II, C. F.; Gezelter, J. D. *J. Am. Chem. Soc.* **2002**, *124*, 11989–11996.

(21) Porter, D. A.; Easterling, K. E. *Phase Trasnformations in Metals and Alloy*, 2nd ed.; Chapman & Hall: London, 1992.

(22) Brust, M.; Walker, M.; Bethell, D.; Schiffrin, D. J.; Whyman, R. *J. Chem. Soc. Chem. Commun.* **1994**, 801–802.

(23) Bao, Y.; Calderon, H.; Krishnan, K. M. *J. Phys. Chem. C* **2007**, *111*, 1941–1944.

(24) Bao, Y.; Krishnan, K. M. *Jour. Mag. Mag. Mater.* **2005**, *293*, 15–19.

(25) Bao, Y.; Pakhomov, A. B.; Krishnan, K. M. *J. Appl. Phys.* **2005**, *97*, 10J317.

(26) Kim, B. Y.; Shim, I. B.; Araci, Z. O.; Saavedra, S. S.; Monti, O. L. A.; Armstrong, N. R.; Sahoo, R.; Srivastava, D. N.; Pyun, J. *J. Am. Chem. Soc.* **2010**, *132*, 3234–3235.

(27) Massalki, T. B. *Binary Alloy Phase Diagrams*, 2nd ed.; Massalski, T. B., Okamoto, H., Subramanian, P. R., Kacprak, L., Eds.; ASM International: Metals Park, OH, 1990; pp 346−348; pp 835−836.

(28) Shevchenko, E. V.; Bodnarchuk, M. I.; Kovalenko, M. V.; Talapin, D. V.; Smith, R. K.; Aloni, S.; Heiss, W.; Alivisatos, P. A. *Adv. Mater.* **2008**, *20*, 4323–4329.

(29) Yin, J. S.; Wang, Z. L. *J. Phys. Chem. B* **1997**, *101*, 8979–8983.

(30) Banhart, F.; Hernández, E.; Terrones, M. *Phys. Rev. Lett.* **2003**, *90*, 185502.

(31) Eshelby, J. D. *Proc. R. Soc. London, Ser. A* **1957**, *241*, 376–396. **1959**, *252*, 561−569.

(32) Duan, H. L.; Jiao, Y.; Yi, X.; Huang, Z. P.; Wang, J. *J. Mech. Phys. Solids* **2006**, *54*, 1401–1425.

(33) Gertsman, V. Y.; Birringer, R. *Scripta Metal. Mater.* **1994**, *30*, 577–581.

(34) Wen, T.; Stach, E. A.; Krishnan, K. M. Unpublished.

JP1053666